Soft effective interactions between weakly charged polyelectrolyte chains

M. Konieczny,* C. N. Likos, and H. Löwen

Institut für Theoretische Physik II,

Heinrich-Heine-Universität Düsseldorf,

Universitätsstraße 1, D-40225 Düsseldorf, Germany

(Dated: **February 2, 2008**, submitted to *The Journal of Chemical Physics*)

Abstract

We apply extensive Molecular Dynamics simulations and analytical considerations in order to study the conformations and the effective interactions between weakly charged, flexible polyelectrolyte chains in salt-free conditions. We focus on charging fractions lying below 20%, for which case there is no Manning condensation of counterions and the latter can be thus partitioned in two states: those that are trapped within the region of the flexible chain and the ones that are free in the solution. We examine the partition of counterions in these two states, the chain sizes and the monomer distributions for various chain lengths, finding that the monomer density follows a Gaussian shape. We calculate the effective interaction between the centers of mass of two interacting chains, under the assumption that the chains can be modeled as two overlapping Gaussian charge profiles. The analytical calculations are compared with measurements from Molecular Dynamics simulations. Good quantitative agreement is found for charging fractions below 10%, where the chains assume coil-like configurations, whereas deviations develop for charge fraction of 20%, in which case a conformational transition of the chain towards a rodlike configuration starts to take place.

PACS numbers: 82.70.-y, 82.35.Rs, 61.20.-p

I. INTRODUCTION

Polyelectrolytes (PE's) are polymer chains that carry ionizable groups along their backbone.[1,2,3] Thereby, when dissolved in a polar solvent such as water, these groups dissociate and a chain that carries charges along its monomer sequence results, leaving behind the dissociated counterions in the solution. Upon addition of salt, additional counterions as well as coions can be found in the system. One deals therefore with a statistical-mechanical problem that entails aspects pertinent to both charge-stabilized colloidal suspensions[4] and polymer solutions. This dual character of polyelectrolytes lies in the heart of the difficulties in devising suitable theoretical approaches to tackle questions regarding their conformations and structure in nonvanishing concentrations. Indeed, the long-range character of the Coulomb interaction renders the typical renormalization-group techniques that have proven very fruitful for neutral polymer chains rather inadequate for the problem at hand. Moreover, the appearance of additional length scales (such as the Bjerrum length, to be defined in what follows) has the consequence that several microscopic parameters have an influence on the physics of the system, in contrast to the case of neutral polymer chains.[3] Simulation approaches, pioneered by the work of Stevens and Kremer,[5,6] have thus proven very useful in shedding light into the question of the typical sizes and conformations of isolated PE chains.

Considerable work has been devoted to the study of sizes, conformations and charge distribution of isolated PE chains under the influence of various physical parameters. These include the effects of counterions and salt,[7] of the temperature,[8] of annealed versus quenched backbone charges[9] as well as of solvent quality.[10,11,12] In the absence of screening, it has been found that the typical size R of a PE chain scales with the degree of polymerization N as $R \sim N(\ln N)^{1/3}$ at room temperature.[13,14] Another issue concerning isolated PE chains that has attracted considerable interest, is that of Manning condensation[15] along the stiff, rodlike backbone. The fraction of condensed counterions has been examined both in theory[16,17] and in experiments.[18,19] Counterion condensation and fluctuations have been shown to lead to a collapse of the rodlike chains, due to the effective monomer-monomer attractions that result from the condensed counterions that position themselves between the charged monomers.[20,21,22,23,24,25]

Relatively less is known about the behavior of polyelectrolyte solutions at finite concentration. Theoretical approaches on this topic are usually based on integral equation theories

that assume rodlike configurations of the chains[26,27,28,29,30] and make use of the polymer reference interaction site model (PRISM) of Schweizer and Curro.[31] An approach that combines aspects from field-theoretical methods and liquid-state theory has been developed by Yethiraj,[32] and which allows for a self-consistent calculation of the solvation potential on a chain, due to the rest of the solution.[33] This theory has been applied to calculate the extent of the PE chains as well as the correlation functions between the monomers at varying concentration, both ignoring[32,33] and including[34,35] the excluded-volume interactions. Recently, phase separation and Coulomb criticality in polyelectrolyte solutions was also studied by means of Monte Carlo computer simulations.[36]

A very useful theoretical tool that greatly facilitates the analysis of the structure and thermodynamics of complex fluids is that of the effective interaction between suitably chosen degrees of freedom that characterize the macromolecule as a whole.[37] For instance, it has been recently shown through extensive computer simulations that neutral polymer chains can be modeled as ultrasoft colloids if their centers of mass are chosen as the effective coordinates that describe the chains in a coarse-grained fashion.[38,39,40] Effective interactions between polyelectrolytes have not been derived up to now, however, with the exception of the case of rodlike molecules.[41] It is the purpose of this paper to fill this gap, by considering *weakly charged* PE chains for which (a) the chains are still flexible and assume a large number of conformations and (b) there are no Manning-condensed counterions. We perform this coarse-graining procedure by tracing out the monomer and counterion degrees of freedom in a salt-free solution and we derive an effective, density-dependent potential of mean force between the centers of mass of the PE chains. Since the analytic considerations for the derivation of the effective interaction are based on knowledge of the sizes and shapes of individual chains, we present first in Sec. II simulation and analytical results pertaining to single polyelectrolytes and demonstrate the good agreement between the two. The theory and the simulation results for the effective potential are presented in Sec. III, whereas in Sec. IV we summarize and conclude. Some technical derivations are shown in the Appendix.

II. SIZES AND CONFORMATIONS OF ISOLATED PE CHAINS

A. Simulation model

We start with the description of our simulation model, valid for both an isolated PE chain and two interacting PE chains. We performed monomer-resolved molecular dynamics simulations (MD). We employed a cubic simulation box with periodic boundary conditions and typical edge lengths in the range $L = 2R_\mathrm{e}$ to $5R_\mathrm{e}$, where R_e is the end-to-end distance of the chain, depending on the other parameters. To integrate the equations of motion, we used the so-called velocity form of Verlet's algorithm.[42,43,44] In order to stabilize the temperature of the system, a Langevin thermostat was applied.[45,46,47] This method is based on the introduction of convenient random and friction forces taking the fluctuation-dissipation theorem into account. The electrostatic Coulomb interaction (see below) of charged particles was treated using Lekner's summation method,[48] where an enhancement of the convergence properties of the associated sums is achieved via their adequate re-writing. Thus, a cut-off becomes feasible. To limit the memory consumption of the tables containing the corresponding forces, we computed the latter by means of a trilinear interpolation,[49] while simultaneously decreasing the number of grid points.

The PE chains were modeled as bead spring chains of N Lennard-Jones (LJ) particles. This method was first introduced in investigations of neutral polymer chains and stars[6,50,51] and turned out to be a reasonable approach. To mimic good solvent conditions, we use a shifted LJ potential to describe the purely repulsive excluded volume interaction of the monomers:

$$V_\mathrm{LJ}(r) = \begin{cases} 4\varepsilon_\mathrm{LJ}\left[\left(\frac{\sigma_\mathrm{LJ}}{r}\right)^{12} - \left(\frac{\sigma_\mathrm{LJ}}{r}\right)^{6} + \frac{1}{4}\right], & r \leq 2^{1/6}\sigma_\mathrm{LJ} \\ 0, & r > 2^{1/6}\sigma_\mathrm{LJ}. \end{cases} \tag{1}$$

Here, r is the spatial distance of two interacting particles. σ_LJ denotes their microscopic length scale, and ε_LJ sets the energy scale for the system. We chose the value $T = \varepsilon_\mathrm{LJ}/k_\mathrm{B}$ for the system's temperature, where k_B is the Boltzmann constant.

The bonds of adjacent monomers were depicted via a finite extension nonlinear elastic

(FENE) potential:[50,51]

$$V_{\mathrm{FENE}}(r) = \begin{cases} -\frac{k_{\mathrm{FENE}}}{2}\left(\frac{R_0}{\sigma_{\mathrm{LJ}}}\right)^2 \ln\left[1-\left(\frac{r}{R_0}\right)^2\right], & r \leq R_0 \\ \infty, & r > R_0, \end{cases} \tag{2}$$

where k_{FENE} is the spring constant. Its value was set to $k_{\mathrm{FENE}} = 7.0\varepsilon_{\mathrm{LJ}}$. The FENE interaction diverges at $r = R_0$, which determines the maximum relative displacement of two neighboring beads. The energy $\varepsilon_{\mathrm{LJ}}$ is the same as in Eq. (1), whereas for the length scale R_0 we have chosen the value $R_0 = 2.0\sigma_{\mathrm{LJ}}$.

Each chain is charged by a fraction α in a periodical manner: every $1/\alpha$ bead carries a monovalent charge. Due to the requirement of electroneutrality, the same amount of also monovalent but oppositely charge ions, namely $N_{\mathrm{c}} = \alpha N$ counterions, are included in the simulation box. They are able to freely move in the box, thereby they had to be simulated explicitly.

Finally, the Coulomb interaction $V_{\mathrm{Coul}}(r)$ between charged particles had to be taken into account. Referring to the valencies of monomer ions and counterions as $q_\alpha = \pm 1$, respectively, the following equation holds:

$$\begin{aligned} \frac{V_{\mathrm{Coul}}(r_{\alpha\beta})}{k_{\mathrm{B}}T} &= \frac{1}{k_{\mathrm{B}}T}\frac{q_\alpha q_\beta e^2}{\epsilon r_{\alpha\beta}} \\ &= \lambda_{\mathrm{B}}\frac{q_\alpha q_\beta}{r_{\alpha\beta}}, \end{aligned} \tag{3}$$

where $r_{\alpha\beta} = |\mathbf{r}_\alpha - \mathbf{r}_\beta|$, with $\mathbf{r}_\alpha$ and $\mathbf{r}_\beta$ denoting the position vectors of particles α and β, respectively. The Bjerrum length is defined as the length at which the electrostatic energy equals the thermal energy:

$$\lambda_{\mathrm{B}} = \frac{e^2}{\epsilon k_{\mathrm{B}}T}, \tag{4}$$

where e is the unit charge and ϵ the permittivity of the solvent. For the case of water at room temperature one obtains $\lambda_{\mathrm{B}} = 7.1$ Å. In this work, we consider salt-free solutions only. Furthermore, the solvent was solely taken into account via its dielectric constant ϵ. The Bjerrum length was fixed to $\lambda_{\mathrm{B}} = 3.0\sigma_{\mathrm{LJ}}$.

The edge length L of the simulation box was set having regard to the simulations' respective parameter combinations to suppress surface effects a priori. The center of mass of the system was fixed in the geometric middle of the box. The typical time step was $\Delta t = 0.005\tau$, with $\tau = \sqrt{m\sigma_{\mathrm{LJ}}^2/\varepsilon_{\mathrm{LJ}}}$ being the associated time unit and m the monomer mass. The counterions were taken to have the same mass and size as the charged monomers.

After a long equilibration time (typically 10^5 time steps), different static quantities were calculated during simulation runs lasting about 5×10^5 time steps. We carried out simulations for charging fractions $\alpha = 0.10$ to 0.20 and degrees of polymerization $N = 50$ to 200. In doing so, systematic predictions concerning the α- and N-dependence of both all relevant conformational properties and the effective interaction became possible.

B. Theory

In the theoretical investigations of the scaling properties of isolated PE chains, we use a mean-field, Flory-type approach, similar to that put forward in Refs. 52, 53 and 54. We consider a dilute, salt-free solution of density $\rho_{\rm chain} = N_{\rm chain}/V$, where $N_{\rm chain}$ denotes the number of chains in the macroscopic volume V. For sake of simplicity, we take all ion species to be monovalent. Within the model, a single chain of total charge Q is depicted as a spherical object of characteristic spatial extent R. The $N_{\rm c}$ counterions form an oppositely charged background, whereas we assume the corresponding density profile to be also spherically symmetric. The typical length scale $R_{\rm W} = (4\pi\rho_{\rm chain}/3)^{-1/3}$ of the counterion distribution is determined by $\rho_{\rm chain}$ alone. Fig. 1 shows a sketch of the situation, with the shaded domains visualizing the relevant length scales of our problem.

In the following steps, we always restrict our problem to the consideration of a single PE chain and its associated counterions. This simplification is convenient, since the $N_{\rm c}$ counterions of total charge $-Q$ assure electro-neutrality. Particular attention has to be paid to the Manning condensation of counterions on the semi-flexible chains.[1,2,15,17] Let b denote the average distance of two adjacent monomer ions along the chain backbone. Condensation takes place when the dimensionless fraction $\lambda_{\rm B}/b$ exceeds unity. The inequality $\lambda_{\rm B}/b < 1$ holds for all our parameter combinations and according to Manning theory condensation effects do not play any role. It should be a reasonable approximation to neglect them completely in what follows. This expectation has been confirmed by our simulations.

Our main goal is to obtain theoretical predictions for the equilibrium expectation value of R. It is determined through minimization of a variational free energy, which reads as

$$\mathcal{F}^{(1)}(R;R_{\rm W}) = U_{\rm H}^{(1)} + F_{\rm el} + F_{\rm int} + S_{\rm c}^{(1)}. \tag{5}$$

Here, $U_{\rm H}^{(1)}$ is a mean-field electrostatic contribution, $F_{\rm el}$ and $F_{\rm int}$ represent the influences

of conformational entropy and self avoidance of the monomers and $S_{\mathrm{c}}^{(1)}$ is the entropic contribution of the counterions. All terms will be described in more detail in what follows.

The electrostatic mean-field energy $U_{\mathrm{H}}^{(1)}$ is given by a Hartree-type expression of the general form

$$U_{\mathrm{H}}^{(1)} = \frac{1}{2\epsilon} \iint \mathrm{d}^3 r \; \mathrm{d}^3 r' \; \frac{\varrho^{(1)}(\mathbf{r}) \varrho^{(1)}(\mathbf{r}')}{|\mathbf{r} - \mathbf{r}'|}, \tag{6}$$

with the local charge density $\varrho^{(1)}(\mathbf{r})$ to be defined below. On purely dimensional grounds, we expect a result that writes as

$$\beta U_{\mathrm{H}}^{(1)} = \frac{N_{\mathrm{c}}^2 \lambda_{\mathrm{B}}}{R} \cdot \vartheta^{(1)} \left(\frac{R}{R_{\mathrm{W}}} \right), \tag{7}$$

with $\beta = 1/k_{\mathrm{B}}T$ denoting the inverse temperature. The shape of the dimensionless function $\vartheta^{(1)}(x)$ depends on the underlying charge distribution $\varrho^{(1)}(\mathbf{r})$ alone.

The elastic contribution F_{el} to the free energy is entropic in nature, written as[55]

$$\beta F_{\mathrm{el}} = \beta F(0) + \frac{3R^2}{2Na^2}, \tag{8}$$

with the equilibrium bond length a and the unimportant constant $F(0)$. It stems from an ideal, i.e., Gaussian approximation of the conformational entropy of the chain. For the additional, non-electrostatic contribution, F_{int}, of the PE chain, arising through self-avoidance, we employ the Flory-type expression[55,56]

$$\beta F_{\mathrm{int}}(R) \sim v_0 \frac{N^2}{2R^3}. \tag{9}$$

Here, v_0 is the so-called excluded volume parameter, whose value has been discussed frequently.[57,58,59] The monomer volume turned out as a good approximation for the case of neutral polymer chains. Without Manning condensation, this guess remains valid for PE chains. Thus we chose $v_0 \approx \sigma_{\mathrm{LJ}}^3$, where we identified the typical monomer length with σ_{LJ}. Finally, the term $S_{\mathrm{c}}^{(1)}$ is an ideal entropic contribution of the form

$$\beta S_{\mathrm{c}}^{(1)} = \int \mathrm{d}^3 r \; \rho_{\mathrm{c}}(r) \left[\ln \left(\rho_{\mathrm{c}}(r) \sigma_{\mathrm{LJ}}^3 \right) - 1 \right] + 3N_{\mathrm{c}} \ln \left(\frac{\Lambda}{\sigma_{\mathrm{LJ}}} \right), \tag{10}$$

where Λ is the thermal de-Broglie wavelength of the counterions. Since $S_{\mathrm{c}}^{(1)}$ is independent of the variational parameter R, it contributes a trivial constant only and will we omitted in all further steps. It was solely included in Eq. (5) for the sake of completeness.

In order to carry out calculations following Eqs. (5) to (9), assumptions concerning the number densities of all ionic particle species are required. On this basis, the total charge

density $\varrho^{(1)}(\mathbf{r})$ can be computed. Due to the small charging fractions α considered here and according to polymer theory,[37,56,60] it is likely to expect a Gaussian shape of the local monomer density $\rho_{\mathrm{m}}(\mathbf{r})$. For the counterions, an adequate approximation remains at first unknown. MD simulations can be helpful to estimate the local densities. Fig. 2 shows corresponding data confirming the above expectations concerning the monomer density profile and proving the absence of any condensation effects. The results regarding the counterion density are ambiguous. Admittedly, the concrete shape of the latter distribution is of minor importance for several reasons: in general, the local arrangement of particles is of secondary relevance when dealing with long-range forces. Since we investigate dilute solutions only, the counterion density remains low anyway. Moreover, without Manning condensation the effective charge of a PE chain equals the bare charge and we expect the monomer ions' contribution to electrostatic energy $U_{\mathrm{H}}^{(1)}$ to be dominant, while the influence of the counterions should be weak. Thus, our main guideline should be to preserve mathematical simplicity. In what follows, we will consider two varying sets of density profiles.

1. Model A: Gaussian monomer density, homogeneous counterion background

Within the scope of a first approach, we postulate a Gaussian monomer density profile according to our MD simulation results

$$\rho_{\mathrm{m}}(\mathbf{r}) = \frac{N}{\pi^{3/2}R^3} e^{-(r/R)^2}, \tag{11}$$

and furthermore assume the counterions to constitute a homogeneously charged background

$$\rho_{\mathrm{c}}(\mathbf{r}) = \frac{N_{\mathrm{c}}\Theta(R_{\mathrm{W}} - r)}{V}, \tag{12}$$

where $\Theta(x)$ is the Heaviside step function. This leads to a total charge density $\varrho^{(1)}(\mathbf{r})$, written as

$$\begin{aligned} \frac{\varrho^{(1)}(\mathbf{r})}{Q} &= \left[\frac{\rho_{\mathrm{m}}(\mathbf{r})}{N} - \frac{\rho_{\mathrm{c}}(\mathbf{r})}{N_{\mathrm{c}}}\right] \\ &= \left[\frac{e^{-(r/R)^2}}{\pi^{3/2}R^3} - \frac{\Theta(R_{\mathrm{W}} - r)}{V}\right]. \end{aligned} \tag{13}$$

Therewith and following Eqs. (6) and (7), we compute the dimensionless function $\vartheta^{(1)}(x)$.

It reads as

$$\vartheta^{(1)}(x) = \frac{1}{\sqrt{2\pi}} + \frac{3x}{5} - 3x^2 \left\{ \frac{e^{-(1/x)^2}}{\sqrt{\pi}} - \left[\frac{x}{2} - \frac{1}{x}\right] \mathrm{erf}\left(\frac{1}{x}\right) \right\}. \tag{14}$$

Summing up all contributions from Eq. (5) yields the total free energy $\mathcal{F}^{(1)}$ of the model system. The value R determining the typical width of the spherical monomer cloud depicting the PE chain is then found by numerical minimization. It acquires an explicit density dependence through R_W, as usual in charged systems.

2. Model B: Gaussian monomer and counterion densities

We now introduce a different modeling of the considered system by replacing the homogeneous counterion background of Sec. II B 1 also with a Gaussian density profile, according to the equation

$$\rho_\mathrm{c}(\mathbf{r}) = \frac{N_\mathrm{c}}{\pi^{3/2} R_\mathrm{W}^3} e^{-(r/R_\mathrm{W})^2}. \tag{15}$$

Regarding the monomer distribution, we still follow the assumptions of the previous section and define the local density $\rho_\mathrm{m}(\mathbf{r})$ using Eq. (11). For the overall charge density $\varrho^{(1)}(\mathbf{r})$ we obtain analogous to Eq. (13):

$$\frac{\varrho^{(1)}(\mathbf{r})}{Q} = \frac{1}{\pi^{3/2}} \left[\frac{e^{-(r/R)^2}}{R^3} - \frac{e^{-(r/R_\mathrm{W})^2}}{R_\mathrm{W}^3} \right]. \tag{16}$$

In anticipation of our considerations for two interacting PE chains [see Eq. (23) in Sec. III A], the following equation must hold:

$$U_\mathrm{H}^{(1)}(R; R_\mathrm{W}) = \frac{1}{2} \lim_{D \to 0} U_\mathrm{H}^{(2)}(D; R; R_\mathrm{W}), \tag{17}$$

where $U_\mathrm{H}^{(2)}(D; R; R_\mathrm{W})$ denotes the electrostatic mean-field contribution to the free energy of two PE chains with center-to-center separation D. Using the results of the Appendix, one finally gets

$$\vartheta^{(1)}(x) = \frac{1}{\sqrt{2\pi}} \left[1 + x - \sqrt{\frac{8}{1 + \left(\frac{1}{x}\right)^2}} \right]. \tag{18}$$

Compared to model A, all steps to come are completely analogous. Once more, minimization results obtained this way exhibit an explicit density dependence via R_W.

TABLE I: Comparison of the chain radii of isolated PE chains obtained from both theory and MD simulation for different monomer numbers N and charging fractions α. The last column lists the number N_c^* of free counterions, necessary to calculate the effective chain interaction at nonoverlapping distances, see Eqs. (27) and (28).

N	α	$(R/\sigma_{LJ})^a$	$(R/\sigma_{LJ})^b$	$(R_g/\sigma_{LJ})^c$	$(R_e/\sigma_{LJ})^c$	$(N_c^*)^c$
50	0.10	10.0	10.2	5.7	14.9	4.8
50	0.20	11.8	12.7	6.6	18.3	8.2
100	0.10	17.2	17.5	10.4	27.1	9.4
100	0.20	22.4	24.4	12.4	34.7	15.0
150	0.10	24.4	24.9	13.9	41.9	13.5
150	0.20	33.3	36.3	21.0	65.6	24.0
200	0.10	31.7	32.5	23.7	65.9	19.4
200	0.20	44.2	48.2	28.9	85.6	34.0

[a] Theory, model A.
[b] Theory, model B.
[c] MD simulation, $N_{chain} = 1$.

C. Comparison to MD results

Based on the mean-field models presented above, predictions of the spatial extent of isolated PE chains become feasible. In order to verify this results, we have to test them against MD data and alternative theoretical approaches. In doing so, we first have to address a somewhat technical question. MD simulations yield expectation values for the radii of gyration R_g and the end-to-end distances R_e, but neither of this quantities strictly corresponds to the variational parameter R as obtained by minimization of the free energy $\mathcal{F}^{(1)}$. Consequently, it remains unclear how a comparison can be carried out. Since we depicted the PE chains as spherical objects, one should expect R to match half the end-to-end distance $R_e/2$. Our results confirm such guess a posteriori, as will be seen shortly.

Fig. 3 shows typical MD snapshots, that give rise to some first conclusions. A variation of the lateral chain extent becomes manifest, i.e., PE chains are more strongly stretched in the mid region than at their ends. This finding is in agreement with the results in Refs. 9

and 14. In general, the spatial configurations of PE chains are determined by two competing contributions to the free energy: the Coulomb repulsion and conformational entropy. For monomer ions in the middle of the chain sequence, electrostatic influences dominate and the described stretching is energetically favorable. But regarding the outermost parts of the chain backbone, the interaction of charged particles is of less importance, while the conformational entropy now becomes deciding. This leads to more coil-like arrangements of the affected monomers. In particular, short chains (monomer number $N \lesssim 50$) remain coiled even for increasing charging fractions α.

While simplified theoretical approaches predict a linear relationship $R \sim N$ between chain radius and monomer number,[25] the effect described above requires some modifications of this scaling law. Considerations based on the concept of so-called electrostatic blobs yield weak logarithmic corrections, resulting in an expression of the general form[9,13,14]

$$R \sim N(\ln N)^{1/3}. \tag{19}$$

Fig. 4 compares MD data with chain radii obtained by both our mean-field theories and the scaling law pursuant to Eq. (19) for two different charging fractions. In the latter case, the unknown constant of proportionality was conveniently determined by means of a fit to the MD results. Thus, theoretical predictions and simulational findings are in good qualitative and quantitative agreement. This agreement particularly improves with increasing degree of polymerization N, because the basic assumption of continuous density profiles in place of an explicit consideration of discrete particles becomes more and more reasonable under these circumstances. Moreover, the presented results confirm our identification of the variational parameter R with half the end-to-end distance $R_\mathrm{e}/2$. Here, we want to point out that the radius of gyration is noticeably smaller (see Tab. I).

In addition, Figs. 4 and 5 directly offer a possibility to read off information concerning the charge dependence of the spatial conformations of PE chains. According to this, in the event of very short chains, the chain radii are approximately unaffected by the charging fraction α. Effects due to the Coulomb repulsion of equally charged beads do not clearly manifest themselves until the monomer number increases noticeably. Then, with increasing α, a transition from coil-like to rod-like configurations takes place. In other words, for fixed N, the spatial extent of such chains is monotonously ascending with the charging fraction. Deviations from this behavior are likely to expect for highly charged chains only. Under

these conditions, Manning condensation becomes more relevant and causes a collapse back to coil-like conformations.[1,2,25,61] However, for the range of parameters considered here, we do not have to take such processes into account, as our simulations unambiguously prove.

III. EFFECTIVE INTERACTIONS BETWEEN PE CHAINS

A. Theory

To derive a theoretical model for the effective interaction $V_{\text{eff}}(D)$ of two PE chains, we separately consider the cases of small ($D \leq D_0$) and large ($D > D_0$) distances of their centers of mass, respectively. The approach we apply is motivated by similar investigations for polymer and PE stars,[54,62] where an overlap condition for two stars of radius R_{star} determines the parameter $D_0 = 2R_{\text{star}}$. But here, the linear chains we deal with are fractal objects of a certain flexibility. Thus, the notion of chain overlap in the previous sense becomes meaningless. The latter fact strongly affects our modeling. According to this, the requirement of continuity of the effective potential and the corresponding force when matching the partial solutions $V_{\text{eff}}^{-}(D)$, valid for $D \leq D_0$, and $V_{\text{eff}}^{+}(D)$, valid for $D > D_0$, defines the value of D_0. In particular, D_0 varies depending on the set of parameters considered.

At first, we assume distances $D \leq D_0$. The effective interaction $V_{\text{eff}}^{-}(D)$ results after taking a canonical trace over all but the chain center of mass degrees of freedom. Let $\mathcal{F}^{(2)}(z)$ be the Helmholtz free energy of a systems containing two PE chains at center-to-center separation z, therewith follows[37]

$$V_{\text{eff}}^{-}(D) = \mathcal{F}^{(2)}(D) - \mathcal{F}^{(2)}(\infty). \tag{20}$$

The term $\mathcal{F}^{(2)}(\infty)$ is manifestly independent of D and contributes an additive constant only. On this account, it does not affect the effective forces, which are obviously obtained by deriving the effective potential with respect to D, i.e., using the equation $F_{\text{eff}}(D) = -\partial V_{\text{eff}}^{-}/\partial D$. Hence, we drop it in all steps to come.

To calculate the Helmholtz free energy $\mathcal{F}^{(2)}(D)$, we start from a mean-field approach analogous to Sec. II B 2 and model the system of interacting PE chains by superposing two charge density profiles $\varrho^{(1)}(\mathbf{r})$ as given via Eq. (16). In other words, we assume them to maintain the same profiles as in the case of isolated chains and to completely interpenetrate, whereby both charge distributions are shifted with respect to each other by the vector $\mathbf{D}$

connecting the chains' centers of mass (see Fig. 6). Moreover, we expect the parameter R to be independent of the center-to-center separation D. Again, the characteristic length scale R_{W} is determined by the density ρ_{chain} directly, i.e., by the equation $R_{\mathrm{W}} = (4\pi\rho_{\mathrm{chain}}/3)^{-1/3}$. As can be seen in Fig. 7, the radii of the chains remain essentially unchanged even at full overlap. Moreover, in Fig. 8 we show the monomer density profiles, averaged over both chains. These are measured during the MD runs as a function of the distance from their common center of mass, for various separations D between the centers of mass of the two chains. It can bee seen that for distances D as small as $10\sigma_{\mathrm{LJ}}$, the individual profiles can still be described by Gaussian functions. Consequently, the overall charge density $\varrho^{(2)}(\mathbf{r};\mathbf{D})$ reads as

$$\varrho^{(2)}(\mathbf{r};\mathbf{D}) = \varrho^{(1)}(\mathbf{r}) + \varrho^{(1)}(\mathbf{r}-\mathbf{D}). \tag{21}$$

By now, we are interested in the effective interaction as a function of the center-to-center separation D exclusively, whereas conformational properties should not be considered. Thus, contrary to Sec. II B, we omit any minimization of the free energy. Instead, we use the width R of the monomer density profiles as additional fit parameter. As we will see, optimal agreement between theoretical predictions and MD data is achieved when R approximately matches half the end-to-end distance $R_{\mathrm{e}}/2$ of isolated PE chains (see Tab. II).

In what follows, we completely neglect the conformational entropy F_{el} and excluded volume interaction F_{int}, which are only weakly dependent on the inter-chain distance D. Hence, they yield constant contributions only and do not influence the effective potential $V_{\mathrm{eff}}(D)$ significantly. Our problem immediately reduces to the computation of electrostatic term $U_{\mathrm{H}}^{(2)}(D)$ and counterion entropy $S_{\mathrm{c}}^{(2)}(D)$, i.e., we have

$$\mathcal{F}^{(2)}(D;R;R_{\mathrm{W}}) = U_{\mathrm{H}}^{(2)}(D) + S_{\mathrm{c}}^{(2)}(D). \tag{22}$$

Taking Eqs. (16) and (21) into account, we are able to conveniently rewrite Eq. (6). Dropping all irrelevant D-independent self energy terms, we obtain

$$U_{\mathrm{H}}^{(2)}(D) = \frac{1}{\epsilon}\iint \mathrm{d}^3r\ \mathrm{d}^3r'\ \frac{\varrho^{(1)}(\mathbf{r})\varrho^{(1)}(\mathbf{r}'-\mathbf{D})}{|\mathbf{r}-\mathbf{r}'|}. \tag{23}$$

On purely dimensional grounds, the result of the above integration must read as (cf. Sec. II B)

$$\beta U_{\mathrm{H}}^{(2)}(D) = \frac{N_c^2\lambda_{\mathrm{B}}}{D}\cdot\vartheta^{(2)}\left(\frac{R}{D},\frac{R_{\mathrm{W}}}{D}\right). \tag{24}$$

Once more, the specific shape of the dimensionless function $\vartheta^{(2)}(x)$ depends on the underlying charge densities $\varrho^{(1)}(\mathbf{r})$ and $\varrho^{(2)}(\mathbf{r})$ alone. A detailed derivation in case of Gaussian density profiles for each chain and for the associated counterions (Model B) according to Eq. (16) of Sec. II B 2 is presented in the Appendix. The corresponding result reads as

$$\vartheta^{(2)}\left(\frac{R}{D},\frac{R_{\mathrm{W}}}{D}\right)=h\left(\frac{R^2}{2D^2}\right)+h\left(\frac{R_{\mathrm{W}}^2}{2D^2}\right)-2h\left(\frac{R^2+R_{\mathrm{W}}^2}{4D^2}\right), \tag{25}$$

where we introduced the abbreviation

$$h(x)=\frac{2}{\pi}\int_0^\infty \mathrm{d}t\,\frac{\sin(t)}{t}e^{-t^2x}. \tag{26}$$

Since an analytical computation of both $h(x)$ and the counterion entropy $S_{\mathrm{c}}(D)$ is not feasible, we need to make use of numerical methods,[49] starting from Eqs. (10), (16) and (21). By means of this, the Helmholtz free energy $\mathcal{F}_2(D;R;R_{\mathrm{W}})$ and the effective potential $V_{\mathrm{eff}}^{-}(D)$ are known in principle. They exhibit a typical explicit density dependence via R_{W}. The corresponding forces must inherit such property, what has to be regarded during any comparison to MD data.

Fig. 9 quantitatively compares the parts $U_{\mathrm{H}}^{(2)}(D)$ and $S_{\mathrm{c}}^{(2)}(D)$ for an exemplary chosen parameter combination. It can be seen that their variations with D, which determines the effective force through the D-derivative of these contributions, are comparable, i.e., neither of them dominates the physics of our system over the other. This is contrary to comparable results for PE stars,[54] where the electrostatic energy constitutes the major influence for small arm numbers f, while it is of minor importance for the opposite case of big f. For the latter situation, the PE stars nearly act as if the were neutral, due to the strong adsorption of counterions in their interior,[53,54] a mechanism absent in the case of PE chains at hand.

Now, the case of inter-chain distances $D > D_0$ has to be considered. We assume the chains to be spheres of average radius R_{g}, whose respective net charges $Q^*=N_{\mathrm{c}}^*e$ are reduced compared to the bare charges $Q=N_{\mathrm{c}}e$ due to counterions located within this spheres. Each chain is surrounded by a cloud of the remaining N_{c}^* free counterions, which cause an additional electrostatic screening of the interaction. Again, $R_{\mathrm{W}}=(4\pi\rho_{\mathrm{chain}}/3)^{-1/3}$ denotes the clouds' characteristic spatial extent.

Adopting a Debye-Hückel approach[4] for nonoverlapping polyelectrolytes, we postulate a Yukawa-type expression for the effective interaction potential there, i.e.,

$$\beta V_{\mathrm{eff}}^{+}(D)=N_{\mathrm{c}}^2\lambda_{\mathrm{B}}\frac{e^{-D/\lambda_{\mathrm{D}}}}{D}. \tag{27}$$

Here, the screening length λ_D is mainly determined by the radii R_g of the spheres and the number N_c^* of free counterions. We obtain[37]

$$\lambda_\mathrm{D} = \left[\frac{R_\mathrm{W}^3 - R_\mathrm{g}^3}{3 N_\mathrm{c}^* \lambda_\mathrm{B}} \right]^{1/2} . \tag{28}$$

In what follows, we fix both R_g and N_c^* according to MD results (see Tab. I). Thereby, the latter is determined by calculating the time average of the number of counterions within an imaginary sphere around a single chain's center of mass whose radius equals the instantaneous value of the corresponding radius of gyration. In doing so, we know the mean net charge Q^* at the same time. There are no further fit parameters, i.e., the Yukawa tail $V_\mathrm{eff}^+(D)$ of the effective potential is completely specified by Eqs. (27) and (28). It exhibits explicit and implicit density dependences via the quantities R_W and N_c^*, respectively.

In order to determine the interval boundary D_0, we simply introduce a continuity constraint for the effective force $F_\mathrm{eff}(D) = -\partial V_\mathrm{eff}(D)/\partial D$. In mathematical formulation, the corresponding condition reads as

$$\left. \frac{\partial \left[V_\mathrm{eff}^-(D) - V_\mathrm{eff}^+(D) \right]}{\partial D} \right|_{D_0} = 0. \tag{29}$$

The final step in deriving the total potential $V_\mathrm{eff}(D)$ is to match both parts of the function at $D = D_0$. This is feasible by constantly shifting $V_\mathrm{eff}^-(D)$ only, since $V_\mathrm{eff}(D)$ must vanish for increasing chain separations $D \to \infty$. Thus, the following definition is convenient:

$$V_\mathrm{eff}(D) = \begin{cases} V_\mathrm{eff}^-(D) + V_\mathrm{eff}^+(D_0) - V_\mathrm{eff}^-(D_0), & D \leq D_0 \\ V_\mathrm{eff}^+(D), & D > D_0 \end{cases} . \tag{30}$$

Fig. 10 shows corresponding results for several parameter combinations. The effective interaction is purely repulsive in nature, ultra-soft and even bounded for vanishing distances $D \to 0$. There is a strong charge dependence of the potential, i.e., changing the charging fraction from $\alpha = 0.10$ to $\alpha = 0.20$ roughly yields a factor two. To emphasize the latter fact, Fig. 10(c) additionally includes an effective potential $V_\mathrm{eff}^{(0)}$ for neutral polymer chains, which was computed using the equation[39]

$$\beta V_\mathrm{eff}^{(0)}(D) = 1.87 \cdot \exp \left[- \left(\frac{D}{1.13 \cdot R_\mathrm{g}} \right)^2 \right] . \tag{31}$$

Compared to charged systems, the neutral polymer effective interaction is about two orders of magnitude weaker. Within the scope of our considerations, we did not investigate the explicit and implicit density dependences of the effective interaction potential in more detail.

B. Comparison to MD results

Now, our theoretical model has to be tested against MD results. A straightforward comparison is not feasible, since (effective) interaction potentials are not accessible directly using standard (MD) simulation techniques. By means of the expressions

$$\begin{aligned}\mathbf{F}_{\alpha}^{(\mathrm{m})}(\mathbf{r}_{1i_0},\mathbf{r}_{2i_0}) &= -\nabla_{\mathbf{r}_{\alpha i_0}} V_{\mathrm{eff}}(\mathbf{r}_{1i_0},\mathbf{r}_{2i_0}) \\ &= \langle \mathbf{f}_{\alpha i_0} \rangle_D \\ &= \mathbf{F}_{\alpha}^{(\mathrm{m})}(D) \end{aligned} \tag{32}$$

and

$$\begin{aligned}\mathbf{F}_{\alpha}^{(\mathrm{c})}(\mathbf{R}_1,\mathbf{R}_2) &= -\nabla_{\mathbf{R}_{\alpha}} V_{\mathrm{eff}}(\mathbf{R}_1,\mathbf{R}_2) \\ &= \left\langle \sum_{i=1}^{N} \mathbf{f}_{\alpha i} \right\rangle_D \\ &= \mathbf{F}_{\alpha}^{(\mathrm{c})}(D), \end{aligned} \tag{33}$$

respectively, we can measure the mean forces acting on given monomers i_0 or the centers of mass. Here, let $\mathbf{f}_{\alpha i}$ be the instantaneous force that monomer i of chain α experiences and $\mathbf{r}_{\alpha i}$ the corresponding spatial position. In addition, the vectors $\mathbf{R}_{\alpha}$ denote the chains' respective centers of mass. In both equations above, $\langle \ldots \rangle_D$ denotes an averaging with fixed chain distance $D = |\mathbf{r}_{1i_0} - \mathbf{r}_{2i_0}|$ or $D = |\mathbf{R}_1 - \mathbf{R}_2|$. For symmetry reasons, the following relation must hold:

$$\mathbf{F}_1^{(\mathrm{m,c})}(D) = -\mathbf{F}_2^{(\mathrm{m,c})}(D) \tag{34}$$

While the validity of Eq. (32) is manifest, Eq. (33) needs a mathematical proof, described in detail in Ref. 63. In all further steps, we consider the magnitude of the force. It is connected to the potential via

$$\begin{aligned} F_{\mathrm{eff}}(D) &= \left| \mathbf{F}_{1,2}^{(\mathrm{m,c})}(D) \right| \\ &= -\frac{\partial V_{\mathrm{eff}}}{\partial D}. \end{aligned} \tag{35}$$

According to this, predictions for the effective forces become computable starting from theoretical results for the corresponding potential. This allows the desired comparison to MD data in principle.

Choosing the centers of mass as effective coordinates is arbitrary; one could have picked, e.g., the central monomers as representatives of the whole chain. The concrete choice of effective coordinates does affect the effective force, as physically expected. However, once the separation between the centers of mass or the central monomers exceeds the typical chain size, it is reasonable to expect that it should be largely irrelevant which degrees of freedom are kept fixed, since the chains appear at these scales as diffuse objects. The latter assumption has been confirmed by our MD simulations. Following this argument, we limit ourselves to the consideration of the centers of mass as effective coordinates according to Eq. (33).

The mean-field model presented in Sec. III A predicts ultra-soft and even bounded effective potentials $V_{\text{eff}}(D)$ (Fig. 10). Thus, the corresponding forces reach their respective maxima at inter-chain distances $D/R_{\text{g}} > 0$, which is in good quantitative agreement with MD results. Fig. 12 shows a concluding comparison of theoretical results and MD data for various parameter combinations. For the lower charge fraction, $\alpha = 0.10$, we find good agreement between theory and simulation, although we observe qualitative deviations for very small inter-chain distances. There, the theoretically predicted forces are in part stronger and, in particular, do not drop to zero for $D/R_{\text{g}} \to 0$, as one would expect on symmetry grounds. This discrepancy is due to the use of Gaussian density profiles (cf. Sec. III A), since such approximation becomes unreasonable for vanishing chain separations (see Fig. 8). The quality of the theory decreases for the larger value of charge fraction, $\alpha = 0.20$, since the chains in this case become more stretched and the underlying theoretical assumption of a Gaussian monomer profile starts losing its validity. Here, modeling the chains as rods would probably yield better results, although these rods are not completely stiff, i.e., pronounced lateral fluctuations are still present. For all plots, values of the fit parameter R (in case $D \leq D_0$) are explicitly given. They roughly equal the half of the end-to-end distances R_{e} of the chains, as measured within simulations (cf. Tab. I). This again allows an interpretation of R as spatial extent of the PE chains and establishes the consistency of the approach for the effective interaction with that for the isolated chains.

The interval boundary D_0 is identifiable by means of a slight cusp in the force vs. distance curves. The latter is not physically reasonable, but an artifact arising as consequence of the matching of both branches. Without the introduction of at least one additional fit parameter, such effect is not avoidable. Our results exhibit a distinct charge dependence of D_0. While

TABLE II: Comparison of the fit parameter R to the chain radii of isolated PE chains as obtained by MD simulation for different monomer numbers N and charging fractions α.

N	α	$(R/\sigma_{\rm LJ})^a$	$(R_{\rm g}/\sigma_{\rm LJ})^b$	$(R_{\rm e}/2\sigma_{\rm LJ})^b$
50	0.10	6.1	5.7	7.5
50	0.20	9.0	6.6	9.2
100	0.10	12.7	10.4	13.6
100	0.20	20.5	12.4	17.4
150	0.10	19.4	13.9	21.0
150	0.20	31.4	21.0	32.8
200	0.10	24.7	23.7	33.0
200	0.20	44.0	28.9	42.8

[a]Theory.
[b]MD simulation, $N_{\rm chain} = 1$.

$D_0/R_{\rm g} \approx 2$ holds for $\alpha = 0.10$ and independent of the monomer number N, the position of the matching moves towards bigger distances $D_0/R_{\rm g} \approx 4$ for $\alpha = 0.20$ and arbitrary N.

IV. SUMMARY AND CONCLUSIONS

We have presented a theoretical approach in describing the conformations and sizes of polyelectrolyte chains. The theory is based on the assumption of Gaussian monomer- and counterion-profiles around the chain's center of mass and employs a variational free energy that includes electrostatic, excluded-volume and entropic contributions. By direct comparison with simulation results, we have shown that the theory is capable of predicting the typical size of PE chains that are weakly charged and its dependence on the charge fraction and the degree of polymerization. Thereafter, the theory has been extended to describe two interacting polyelectrolytes and the effective interaction potential between their centers of mass has been derived and compared successfully with computer simulation results. In doing so, we have made a first step in describing polyelectrolytes as soft colloids, in analogy with recently developed approaches for neutral polymers.[38,39,40] The effective potentials obtained are ultrasoft and bounded but nevertheless much more repulsive than those obtained

for polymer chains. The physical reasons lie both in the electrostatic repulsion between the charges carried on the chains and on the entropically caused osmotic pressure of the counterions that are trapped within the interior of the chains.

The effective potential includes an explicit density dependence arising from the redistribution of counterions inside and outside the chains upon a change of the overall concentration. In principle, this potential can be employed in order to study the structural characteristics of concentrated solutions of polyelectrolytes, i.e., the correlations between the centers of mass of the chains. Moreover, it can be used for the calculation of thermodynamic properties of concentrated solutions, such as free energies and pressure and of phase transitions, such as the phase separation investigated recently by computer simulations.[36] Indeed, whereas it has been already shown that the approach of coarse-graining successfully predicts phase separation in polymer blends,[64] the question of whether the same is true for polyelectrolytes has not been examined to date. We plan to return to this problem in the future.

Acknowledgments

We thank Arben Jusufi, René Messina, Norman Hoffmann and Christian Mayer for helpful discussions. Financial support from the DFG (SFB TR6) is acknowledged.

APPENDIX: PROOF OF EQ. (25)

In Secs. II and III, we dropped technical details of the calculation of the Helmholtz free energies. Here, we want to carry out the derivation of the mean-field contribution $U_{\mathrm{H}}^{(2)}(D)$ for interacting PE chains (cf. Sec. III A) explicitly. We start from the equation

$$U_{\mathrm{H}}^{(2)}(D) = \frac{1}{2\epsilon} \iint \mathrm{d}^3 r \; \mathrm{d}^3 r' \; \frac{\varrho^{(2)}(\mathbf{r};\mathbf{D})\varrho^{(2)}(\mathbf{r}';\mathbf{D})}{|\mathbf{r}-\mathbf{r}'|}. \tag{A.1}$$

Using (21) in (A.1) and neglecting all irrelevant self-energy terms, which are independent of D, we get

$$U_{\mathrm{H}}^{(2)}(D) = \frac{1}{\epsilon} \iint \mathrm{d}^3 r \; \mathrm{d}^3 r' \; \frac{\varrho^{(1)}(\mathbf{r})\varrho^{(1)}(\mathbf{r}'-\mathbf{D})}{|\mathbf{r}-\mathbf{r}'|}. \tag{A.2}$$

Let $*$ denote a convolution of two functions. With the definition $v(r) = 1/(\epsilon r)$, we rewrite (A.2) obtaining

$$\begin{aligned} U_{\mathrm{H}}^{(2)}(D) &= \int \mathrm{d}^3 r' \; \varrho^{(1)}(\mathbf{r}' - \mathbf{D}) \int \mathrm{d}^3 r \; v(|\mathbf{r} - \mathbf{r}'|) \varrho^{(1)}(\mathbf{r}) \\ &= \int \mathrm{d}^3 r' \; \varrho^{(1)}(\mathbf{r}' - \mathbf{D}) \left[\varrho^{(1)} * v\right](\mathbf{r}) \\ &= \left[\varrho^{(1)} * \left[\varrho^{(1)} * v\right]\right](\mathbf{D}). \end{aligned} \tag{A.3}$$

Now, we pass into Fourier space and thereby introduce the notation $\tilde{f}$ for the associated Fourier transform of a function f. First of all, this yields the relation

$$\left[\varrho^{(1)} * v\right](\mathbf{r}) = \frac{1}{(2\pi)^3} \int \mathrm{d}^3 k \; \tilde{\varrho}^{(1)}(\mathbf{k}) \tilde{v}(\mathbf{k}) e^{\mathrm{i}\mathbf{k}\cdot\mathbf{r}}. \tag{A.4}$$

Taking (A.4) into account, (A.3) reads as

$$\begin{aligned} U_{\mathrm{H}}^{(2)}(D) &= \left[\varrho^{(1)} * \left[\varrho^{(1)} * v\right]\right](\mathbf{D}) \\ &= \frac{1}{(2\pi)^3} \int \mathrm{d}^3 k \; \tilde{\varrho}^{(1)}(\mathbf{k}) \widetilde{[\varrho^{(1)} * v]}(\mathbf{k}) e^{\mathrm{i}\mathbf{k}\cdot\mathbf{D}} \\ &= \frac{1}{(2\pi)^3} \int \mathrm{d}^3 k \; \left[\tilde{\varrho}^{(1)}(\mathbf{k})\right]^2 \tilde{v}(\mathbf{k}) e^{\mathrm{i}\mathbf{k}\cdot\mathbf{D}}. \end{aligned} \tag{A.5}$$

With $\varrho^{(1)}(\mathbf{r})/Q = \rho_{\mathrm{m}}(\mathbf{r})/N - \rho_{\mathrm{c}}(\mathbf{r})/N_{\mathrm{c}}$ and regarding the linearity of the Fourier transform, Eq. (A.5) writes as

$$\begin{aligned} U_{\mathrm{H}}^{(2)}(D) =& \frac{Q^2}{(2\pi)^3} \left\{ \frac{1}{N^2} \int \mathrm{d}^3 k \; \tilde{\rho}_{\mathrm{m}}^2(\mathbf{k}) \tilde{v}(\mathbf{k}) e^{\mathrm{i}\mathbf{k}\cdot\mathbf{D}} + \frac{1}{N_{\mathrm{c}}^2} \int \mathrm{d}^3 k \; \tilde{\rho}_{\mathrm{c}}^2(\mathbf{k}) \tilde{v}(\mathbf{k}) e^{\mathrm{i}\mathbf{k}\cdot\mathbf{D}} \right. \\ & \left. - \frac{2}{N N_{\mathrm{c}}} \int \mathrm{d}^3 k \; \tilde{\rho}_{\mathrm{m}}(\mathbf{k}) \tilde{\rho}_{\mathrm{c}}(\mathbf{k}) \tilde{v}(\mathbf{k}) e^{\mathrm{i}\mathbf{k}\cdot\mathbf{D}} \right\}. \end{aligned} \tag{A.6}$$

Up to now, we did not assume any specific properties of the density profiles or the integration kernel v. All considerations are valid in a very general fashion. In our special case, the mentioned functions are radially symmetric. Due to this fact, we obtain

$$\begin{aligned} U_{\mathrm{H}}^{(2)}(D) =& \frac{Q^2}{2\pi^2 D} \left\{ \frac{1}{N^2} \int_0^\infty \mathrm{d}k \; k \sin(kD) \tilde{\rho}_{\mathrm{m}}^2(k) \tilde{v}(k) + \frac{1}{N_{\mathrm{c}}^2} \int_0^\infty \mathrm{d}k \; k \sin(kD) \tilde{\rho}_{\mathrm{c}}^2(k) \tilde{v}(k) \right. \\ & \left. - \frac{2}{N N_{\mathrm{c}}} \int_0^\infty \mathrm{d}k \; k \sin(kD) \tilde{\rho}_{\mathrm{m}}(k) \tilde{\rho}_{\mathrm{c}}(k) \tilde{v}(k) \right\} \\ =& \frac{Q^2}{2\pi^2 D} \left\{ I_1(D) + I_2(D) - 2 I_3(D) \right\} \end{aligned} \tag{A.7}$$

Starting from Eqs. (16), (21) and using the above definition of v, we find

$$\frac{\tilde{\rho}_{\mathrm{m}}(k)}{N} = e^{-k^2R^2/4}, \tag{A.8}$$

$$\frac{\tilde{\rho}_{\mathrm{c}}(k)}{N_{\mathrm{c}}} = e^{-k^2R_{\mathrm{W}}^2/4}, \tag{A.9}$$

$$\tilde{v}(k) = \frac{4\pi}{\epsilon k^2}. \tag{A.10}$$

Based on (A.7) and including Eqs. (A.8) to (A.10), we firstly have as an intermediate result

$$\begin{aligned} I_1(D) &= \frac{4\pi}{\epsilon}\int_0^\infty \mathrm{d}k\, \frac{\sin(kD)}{k} e^{-k^2R^2/2} \\ &= \frac{4\pi}{\epsilon}\int_0^\infty \mathrm{d}t\, \frac{\sin(t)}{t} e^{-t^2(R^2/2D^2)} \\ &= \frac{2\pi^2}{\epsilon}\cdot h\left(\frac{R^2}{2D^2}\right). \end{aligned} \tag{A.11}$$

In complete analogy, we achieve the relations

$$I_2(D) = \frac{2\pi^2}{\epsilon}\cdot h\left(\frac{R_{\mathrm{W}}^2}{2D^2}\right) \tag{A.12}$$

and moreover

$$I_3(D) = \frac{2\pi^2}{\epsilon}\cdot h\left(\frac{R^2+R_{\mathrm{W}}^2}{4D^2}\right). \tag{A.13}$$

For simplicity reasons, we thereby introduced the abbreviated notation

$$h\,(x) = \frac{2}{\pi}\int_0^\infty \mathrm{d}t\, \frac{\sin(t)}{t} e^{-t^2x}. \tag{A.14}$$

Furthermore, we define based on the previous Eqs. (A.11) to (A.13):

$$\begin{aligned} \vartheta^{(2)}\left(\frac{R}{D},\frac{R_{\mathrm{W}}}{D}\right) &= \frac{\epsilon}{2\pi^2}\left\{I_1(D)+I_2(D)-2I_3(D)\right\} \\ &= \left\{h\left(\frac{R^2}{2D^2}\right)+h\left(\frac{R_{\mathrm{W}}^2}{2D^2}\right)-2h\left(\frac{R^2+R_{\mathrm{W}}^2}{4D^2}\right)\right\}. \end{aligned} \tag{A.15}$$

Substituting (A.15) in (A.7) finally yields the result

$$\begin{aligned} \beta U_{\mathrm{H}}^{(2)}(D) &= \frac{\beta Q^2}{\epsilon D}\cdot\vartheta^{(2)}\left(\frac{R}{D},\frac{R_{\mathrm{W}}}{D}\right) \\ &= \frac{N_c^2\lambda_{\mathrm{B}}}{D}\cdot\vartheta^{(2)}\left(\frac{R}{D},\frac{R_{\mathrm{W}}}{D}\right). \end{aligned} \tag{A.16}$$

---

* Electronic address: kon@thphy.uni-duesseldorf.de

[1] F. Oosawa, *Polyelectrolytes* (Marcel Dekker, New York, 1971).

[2] H. Dautzenberg, W. Jaeger, J. Kötz, B. Philipp, Ch. Seidel, and D. Stscherbina, *Polyelectrolytes - Formation, Characterization and Application* (Hanser, München, 1994).

[3] J.-L. Barrat and J.-F. Joanny, Adv. Chem. Phys. **XCIV**, 1 (1995)

[4] J.-P. Hansen and H. Löwen, Ann. Rev. Phys. Chem. **51**, 209 (2000).

[5] M. J. Stevens and K. Kremer, J. Chem. Phys. **103**, 1669 (1995).

[6] M. J. Stevens and K. Kremer, Phys. Rev. Lett. **71**, 2228 (1993).

[7] V. V. Vasilevskaya, A. R. Khokhlov, and K. Yoshikawa, Macromol. Theory Simul. **9**, 600 (2000).

[8] Y. Kantor and M. Kardar, Phys. Rev. Lett. **83**, 745 (1999).

[9] M. Castelnovo, P. Sens and J.-F. Joanny, Eur. Phys. J. E **1**, 115 (2002).

[10] C.-Y. Shew and A. Yethiraj, J. Chem. Phys. **110**, 676 (1999).

[11] U. Micka, C. Holm, and K. Kremer, Langmuir **15**, 4033 (1999).

[12] W. Essafi, F. Lafuma, and C. E. Williams, J. Phys. II (France) **5**, 1269 (1995).

[13] G. Migliorini, V. G. Rostiashvili, and T. A. Vilgis, Eur. Phys. J. E **4**, 475 (2001).

[14] Q. Liao, A. V. Dobrynin, and M. Rubinstein, Macromolecules **36**, 3386 (2003).

[15] G. S. Manning, J. Chem. Phys. **51**, 924 (1969).

[16] R. M. Nyquist, B.-Y. Ha, and A. J. Liu, Macromolecules **32**, 3481 (1999).

[17] M. Deserno, C. Holm, and S. May, Macromolecules **33**, 199 (2000).

[18] J. Blaul, M. Wittemann, M. Ballauff, and M. Rehahn, J. Phys. Chem. B **104**, 7077 (2000).

[19] M. Deserno, C. Holm, J. Blaul, M. Ballauff, and M. Rehahn, Eur. Phys. J. E **5**, 97 (2001).

[20] R. G. Winkler, M. Gold, and P. Reineker, Phys. Rev. Lett. **80**, 3731 (1998).

[21] N. V. Brillantov, D. V. Kuznetsov, and R. Klein, Phys. Rev. Lett. **81**, 1433 (1998).

[22] H. Schiessel and P. Pincus, Macromolecules **31**, 7953 (1998).

[23] H. Schiessel, Macromolecules **32**, 5673 (1999).

[24] R. Golestanian, M. Kardar, and T. B. Liverpool, Phys. Rev. Lett. **82**, 4456 (1999).

[25] R. G. Winkler, in *Soft Matter - Complex Materials on Mesoscopic Scales*, 33. IFF-Ferienkurs, Forschungszentrum Jülich (Jülich, 2002).

[26] A. Yethiraj and C.-Y. Shew, Phys. Rev. Lett. **77**, 3937 (1996).

[27] C.-Y. Shew and A. Yethiraj, J. Chem. Phys. **106**, 5706 (1997).

[28] C.-Y. Shew and A. Yethiraj, J. Chem. Phys. **109**, 5162 (1998).

[29] C.-Y. Shew and A. Yethiraj, J. Chem. Phys. **110**, 11599 (1999).

[30] L. Harnau and P. Reineker, J. Chem. Phys. **112**, 437 (2000).

[31] K. S. Schweizer and J. G. Curro, Adv. Polym. Sci. **116**, 319 (1995).

[32] A. Yethiraj, Phys. Rev. Lett. **78**, 3789 (1997).

[33] A. Yethiraj, J. Chem. Phys. **108**, 1184 (1998).

[34] C.-Y. Shew and A. Yethiraj, J. Chem. Phys. **110**, 5437 (1998).

[35] C.-Y. Shew and A. Yethiraj, J. Chem. Phys. **113**, 8841 (2000).

[36] G. Orkoulas, S. K. Kumar, and A. Z. Panagiotopoulos, Phys. Rev. Lett. **90**, 048303 (2003).

[37] C. N. Likos, Phys. Rep. **348**, 267 (2001).

[38] A. A. Louis, P. G. Bolhuis, J.-P. Hansen, and E. J. Meijer, Phys. Rev. Lett. **85**, 2522 (2000).

[39] A. A. Louis, P. G. Bolhuis, and J.-P. Hansen, Phys. Rev. E **62**, 7961 (2000).

[40] P. G. Bolhuis, A. A. Louis, J.-P. Hansen, and E. J. Meijer, J. Chem. Phys. **114**, 4296 (2001).

[41] G. A. Carri and M. Muthukumar, J. Chem. Phys. **111**, 1765 (1999).

[42] M. P. Allen and D. J. Tildesley, *Computer Simulation of Liquids* (Oxford University Press, Oxford, 1987).

[43] D. Frenkel and B. Smit, *Understandig Molecular Simulation* (Academic Press, San Diego, 1996).

[44] D. C. Rapaport, *The Art of Molecular Dynamics Simulation* (Cambridge University Press, Cambridge, 1995).

[45] K. Kremer and G. S. Grest, J. Chem. Phys. **92**, 5057 (1990).

[46] T. O. White, G. Ciccotti, and J.-P. Hansen, Molec. Phys. **99**, 2023 (2001).

[47] R. Messina, C. Holm, and K. Kremer, J. Chem. Phys. **117**, 2947 (2002).

[48] J. Lekner, Physica A **176**, 485 (1991).

[49] W. H. Press, S. A. Teukolsky, W. T. Vetterling, and B. P. Flannery, *Numerical Recipes in C* (Cambridge University Press, Cambridge, 1995).

[50] G. S. Grest, K. Kremer, and T. A. Witten, Macromolecules **20**, 1376 (1987).

[51] G. S. Grest, Macromolecules **27**, 3493 (1994).

[52] J. Klein Wolterink, F. A. M. Leermakers, G. J. Fleer, L. K. Koopal, E.B. Zhulina, and O.V. Borisov, Macromolecules **32**, 2365 (1999).

[53] A. Jusufi, C. N. Likos, and H. Löwen, Phys. Rev. Lett. 88, 018301 (2002).

[54] A. Jusufi, C. N. Likos, and H. Löwen, J. Chem. Phys. **116**, 11011 (2002).

[55] P. G. de Gennes, *Scaling Concepts in Polymer Physics* (Cornell University Press, Ithaca, 1979).

[56] M. Doi and S. F. Edwards, *The Theory of Polymer Dynamics* (Clarendon Press, Oxford, 1986).

[57] R. Hariharan, C. Biver, J. Mays, and W. B. Russel, Macromolecules **31**, 7506 (1998).

[58] P. Pincus, Macromolecules **24**, 2912 (1991).

[59] T. Odijk and A. H. Houwaart, J. Polym. Sci., Polym. Phys. Ed. **16**, 627 (1978).

[60] M. Doi, *Introduction to Polymer Physics* (Clarendon Press, Oxford, 1996).

[61] S. Liu and M. Muthukumar, J. Chem. Phys. **116**, 9975 (2002).

[62] A. Jusufi, M. Watzlawek, and H. Löwen, Macromolecules **32**, 4470 (1999).

[63] I. O. Götze, H. M. Harreis, and C. N. Likos, J. Chem. Phys. **120**, 7761 (2004).

[64] A. J. Archer, C. N. Likos, and R. Evans, J. Phys.: Condens. Matter **14**, 12031 (2002).

FIGURE CAPTIONS

FIG. 1: A sketch showing a PE chain of typical spatial extent R and the surrounding counterion sphere of radius R_{W}.

FIG. 2: Local number densities of (a) the monomers and (b) of the counterions for an isolated PE chain with $N = 200$, $\alpha = 0.10$ and $R_{\mathrm{W}}/\sigma_{\mathrm{LJ}} = 124.1$, as obtained by MD simulations. Here r denotes the distance from the center of mass of the chain.

FIG. 3: MD snapshots of isolated PE chains with degree of polymerization $N = 200$ and two different charging fractions $\alpha = 0.10$ (left) and $\alpha = 0.20$ (right). Bright gray balls are neutral monomers, and the dark spheres along the chain indicate the charged monomers. The counterions are the small, dark gray spheres around the chain. In addition, the black crosses mark the centers of mass of the instantaneous configurations.

FIG. 4: Spatial extent of isolated PE chains as a function of the degree of polymerization N for charging fractions: (a) $\alpha = 0.10$ and (b) $\alpha = 0.20$. The lines show theoretical results while the symbols denote data obtained by our MD simulations.

FIG. 5: Chain radii of isolated PE chains as a function of the charging fraction α for fixed monomer number $N = 200$ and $R_{\mathrm{W}}/\sigma_{\mathrm{LJ}} = 124.1$, as obtained by our MD simulations.

FIG. 6: A sketch of two overlapping PE chains, for a more detailed explanation of the theoretical modeling, see the text.

FIG. 7: Simulation results for the radii of interacting PE chains, depending on their center of mass separation D. The results shown here refer to parameters $N = 100$ and $\alpha = 0.10$. The corresponding radii of isolated chains are shown as horizontal lines for comparison.

FIG. 8: Density profiles (a) for the monomers and (b) for the counterions of interacting PE chains with $N = 200$, $\alpha = 0.10$, $R_{\mathrm{W}}/\sigma_{\mathrm{LJ}} = 157.6$ and varying center of mass separation D, as obtained via MD simulation.

FIG. 9: Comparison of the terms $U_{\mathrm{H}}^{(2)}(D)$ and $S_{\mathrm{c}}^{(2)}(D)$ that contribute to the Helmholtz free energy as functions of the chain separation D, where we exemplarily chose $N = 200$, $\alpha = 0.10$ and $R_{\mathrm{W}}/\sigma_{\mathrm{LJ}} = 157.6$.

FIG. 10: Theoretically predicted effective potential $V_{\mathrm{eff}}(D)$ as a function of the interchain separation D for (a) $N = 100$, (b) $N = 150$, and (c) $N = 200$. The corresponding charging fractions are $\alpha = 0.10$ and $\alpha = 0.20$, as indicated in the legends. For all cases, the used values of the fit parameter R are specified in the legend boxes. In panel (c) we additionally

show as the dash-dotted line the result valid for neutral polymers.[39]

FIG. 11: Simulation snapshots of interacting PE chains with degree of polymerization $N = 200$ and charging fraction $\alpha = 0.20$. Bright gray balls are neutral monomers, and the dark spheres along the chains indicate the charged monomers. The counterions are the small, dark gray spheres around the chains. The distances of centers of mass, which are marked by the black crosses, are $D = 2\sigma_{\rm LJ}$ (left) and $D = 40\sigma_{\rm LJ}$ (right), respectively. In general, the mean chain directions are not perpendicular to the vector $\mathbf{D}$ connecting the centers of mass.

FIG. 12: The effective force $F_{\rm eff}(D)$ on the center of mass of a polyelectrolyte as a function of the interchain separation D, and for charging fractions $\alpha = 0.10$ [(a), (b), (c)] and $\alpha = 0.20$ [(d), (e), (f)], where the respective degrees of polymerization are: $N = 100$ [(a), (d)], $N = 150$ [(b), (e)], and $N = 200$ [(c), (f)]. Solid lines are theoretical predictions, with the fit parameters R specified in the legend boxes. Data points denote MD results for the chains' centers of mass as reference points.

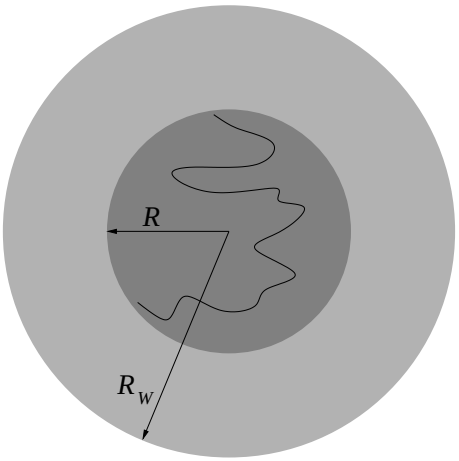

FIG. 1: Konieczny, Likos, Löwen

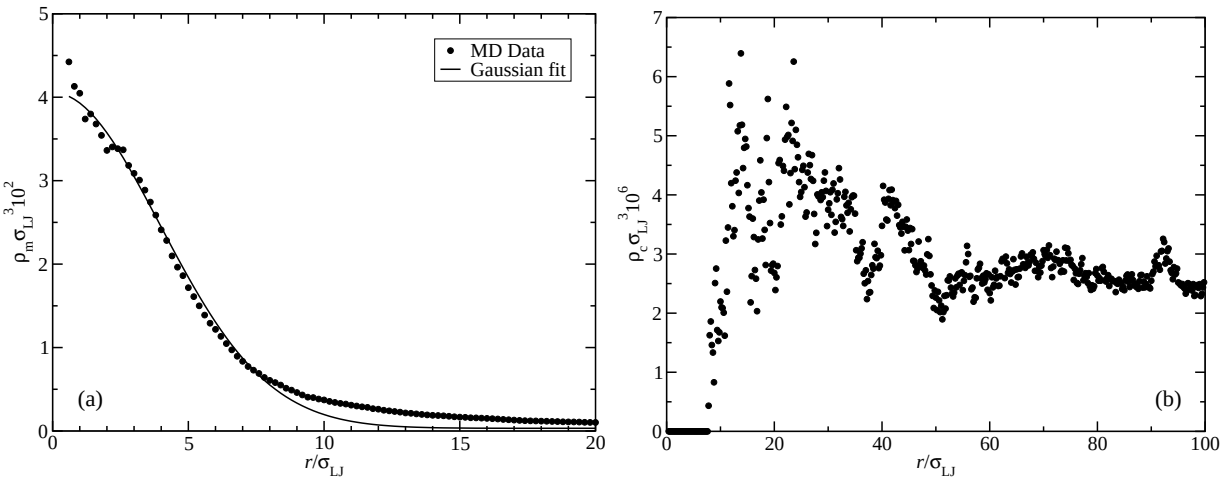

FIG. 2: Konieczny, Likos, Löwen

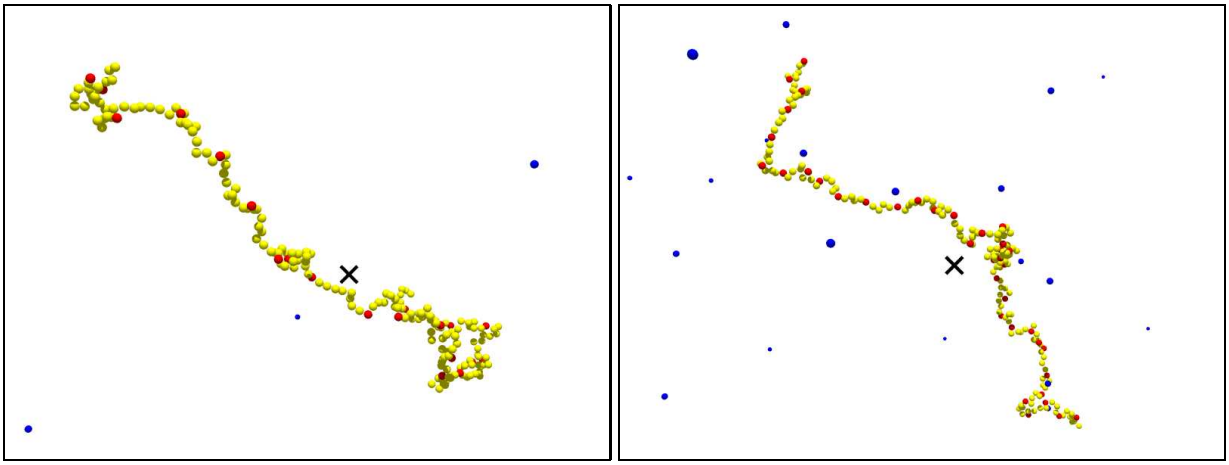

FIG. 3: Konieczny, Likos, Löwen

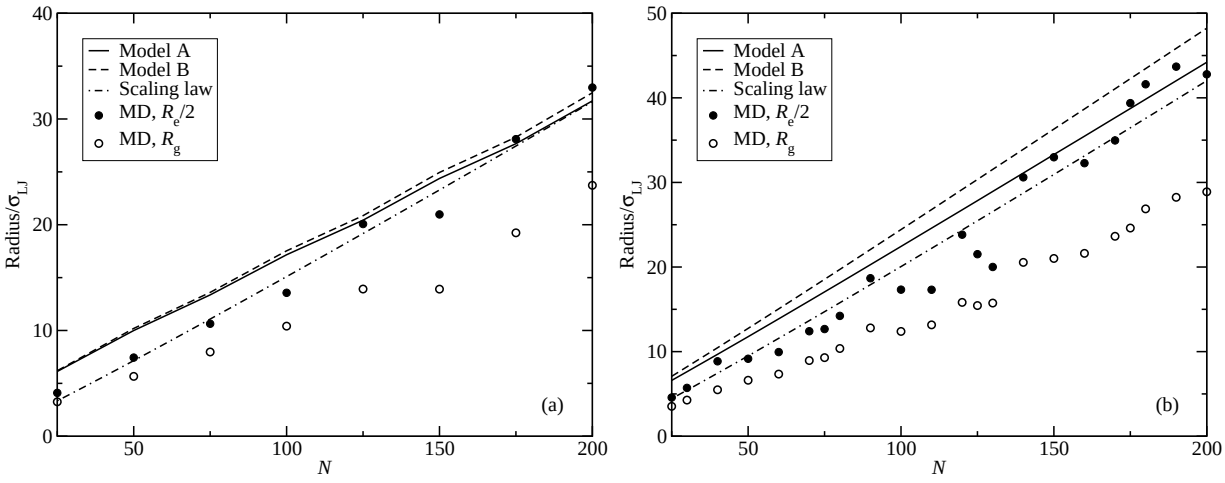

FIG. 4: Konieczny, Likos, Löwen

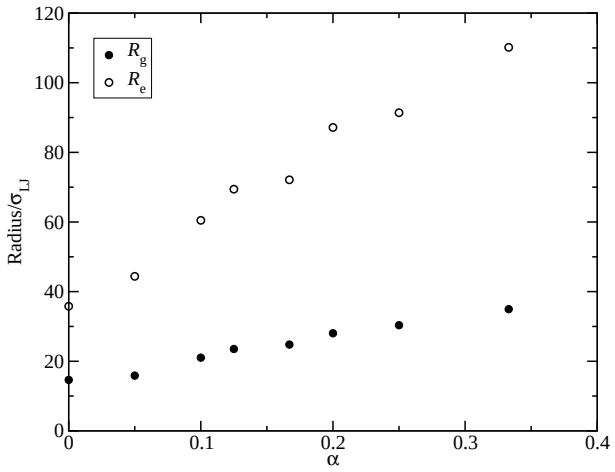

FIG. 5: Konieczny, Likos, Löwen

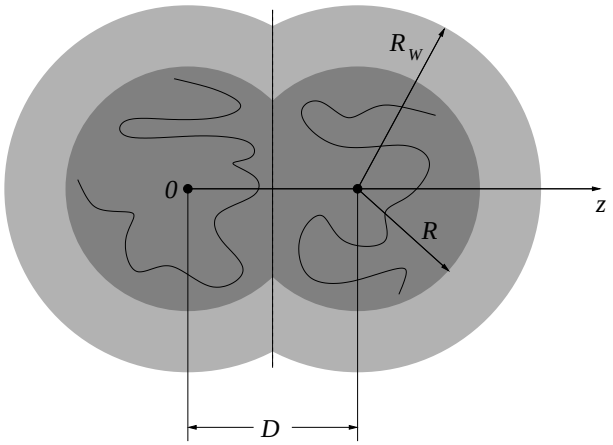

FIG. 6: Konieczny, Likos, Löwen

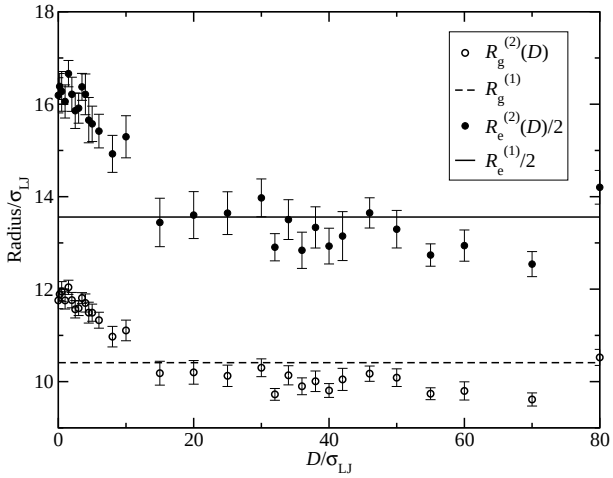

FIG. 7: Konieczny, Likos, Löwen

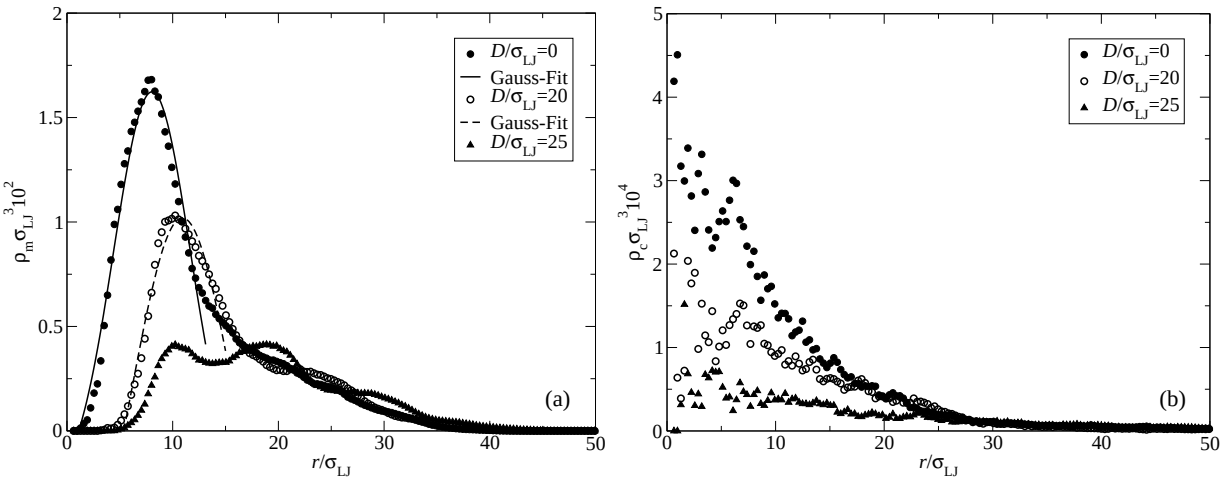

FIG. 8: Konieczny, Likos, Löwen

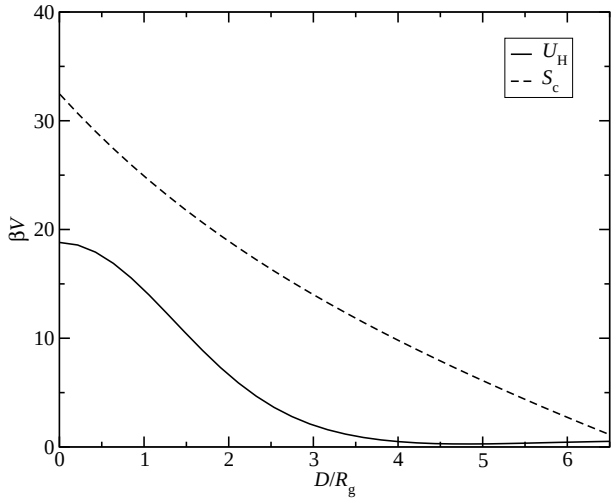

FIG. 9: Konieczny, Likos, Löwen

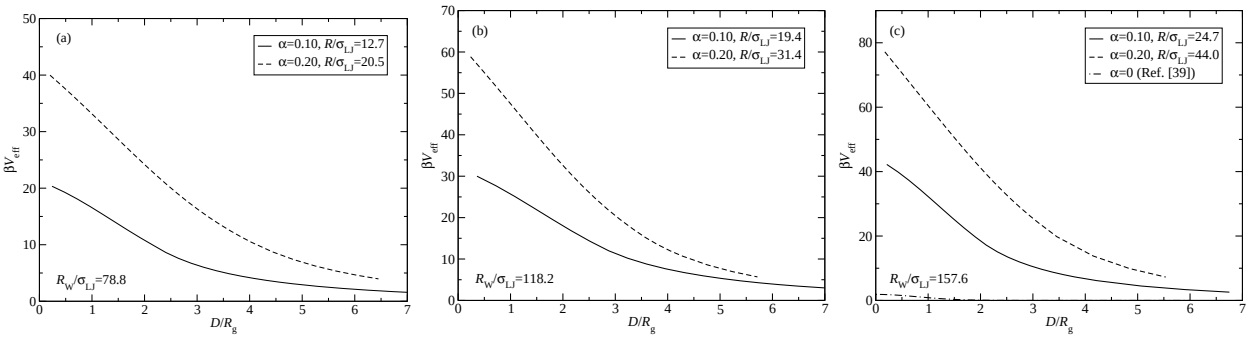

FIG. 10: Konieczny, Likos, Löwen

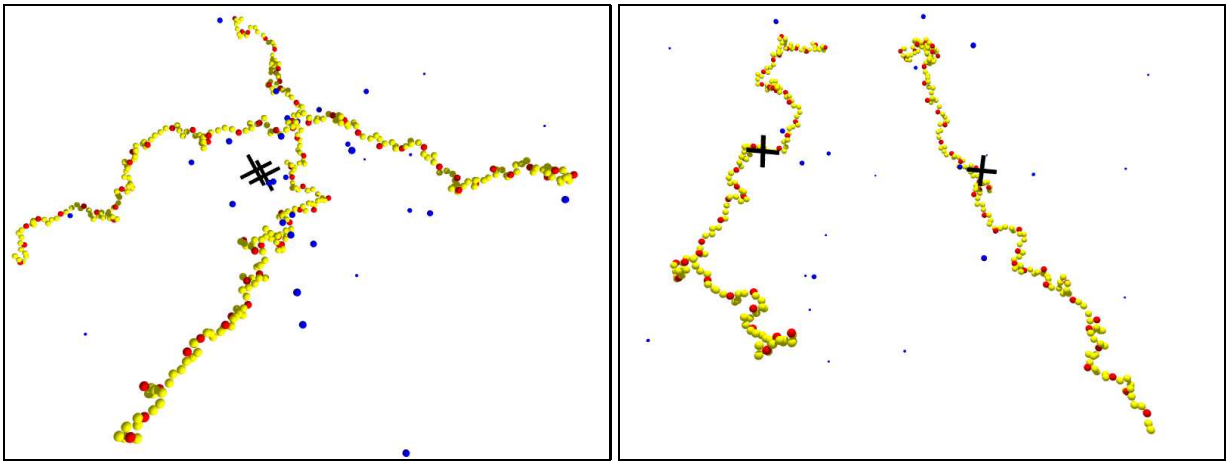

FIG. 11: Konieczny, Likos, Löwen

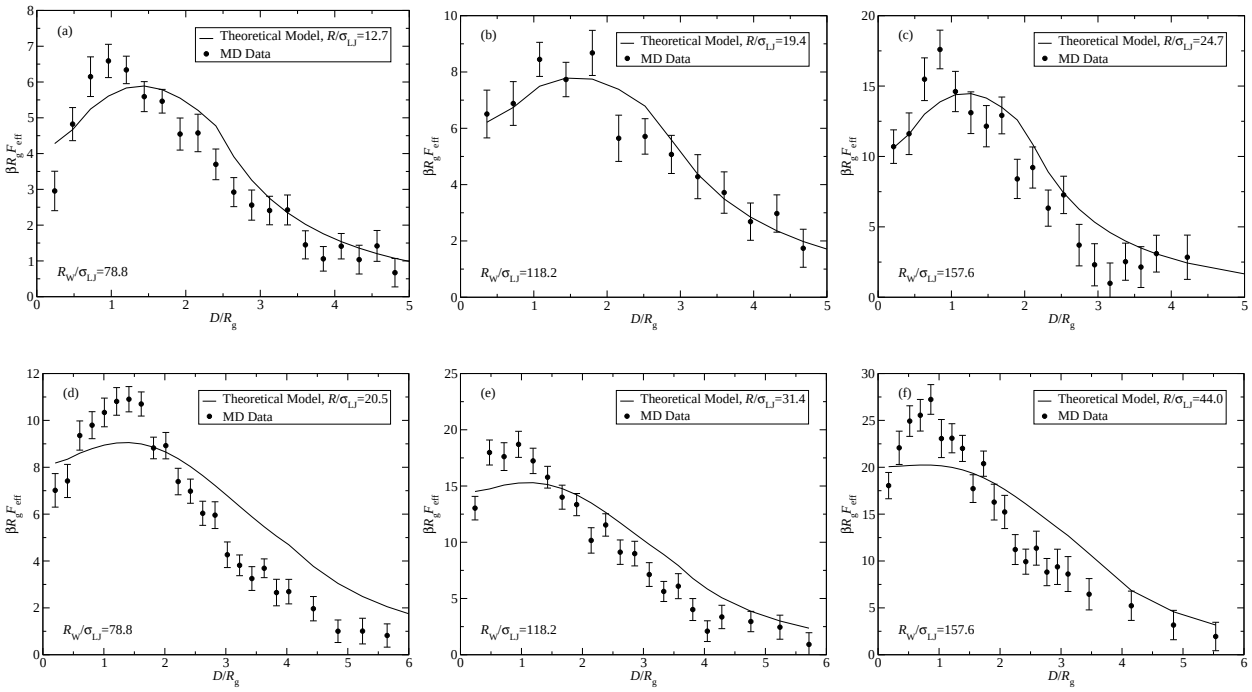

FIG. 12: Konieczny, Likos, Löwen